The Journal of Chemical Physics

Resonances in nitrobenzene probed by the electron attachment to neutral and by the photodetachment from anion

Cite as: J. Chem. Phys. **157**, 064302 (2022); https://doi.org/10.1063/5.0101358
Submitted: 31 May 2022 • Accepted: 15 July 2022 • Published Online: 08 August 2022

Miloš Ranković, Pamir Nag, Cate S. Anstöter, et al.

AIP Publishing

The Journal of Chemical Physics ARTICLE scitation.org/journal/jcp

Resonances in nitrobenzene probed by the electron attachment to neutral and by the photodetachment from anion

Cite as: J. Chem. Phys. 157, 064302 (2022); doi: 10.1063/5.0101358
Submitted: 31 May 2022 • Accepted: 15 July 2022 •
Published Online: 8 August 2022

Miloš Ranković,[1] Pamir Nag,[1] Cate S. Anstöter,[2] Golda Mensa-Bonsu,[2] Ragesh Kumar T. P.,[1] Jan R. R. Verlet,[2,a)] and Juraj Fedor[1,a)]

AFFILIATIONS

[1] J. Heyrovský Institute of Physical Chemistry, Czech Academy of Sciences, Dolejškova 3, 18223 Prague, Czech Republic
[2] Department of Chemistry, Durham University, Durham DH1 3LE, United Kingdom

[a)] **Authors to whom correspondence should be addressed:** j.r.r.verlet@durham.ac.uk and juraj.fedor@jh-inst.cas.cz

ABSTRACT

We probe resonances (transient anions) in nitrobenzene with the focus on the electron emission from these. Experimentally, we populate resonances in two ways: either by the impact of free electrons on the neutral molecule or by the photoexcitation of the bound molecular anion. These two excitation means lead to transient anions in different initial geometries. In both cases, the anions decay by electron emission and we record the electron spectra. Several types of emission are recognized, differing by the way in which the resulting molecule is vibrationally excited. In the excitation of specific vibrational modes, distinctly different modes are visible in electron collision and photodetachment experiments. The unspecific vibrational excitation, which leads to the emission of thermal electrons following the internal vibrational redistribution, shows similar features in both experiments. A model for the thermal emission based on a detailed balance principle agrees with the experimental findings very well. Finally, a similar behavior in the two experiments is also observed for a third type of electron emission, the vibrational autodetachment, which yields electrons with constant final energies over a broad range of excitation energies. The entrance channels for the vibrational autodetachment are examined in detail, and they point to a new mechanism involving a reverse valence to non-valence internal conversion.

I. INTRODUCTION

Electron–molecule resonances, or transient anions, are interesting species from the fundamental point of view of nuclear dynamics. The total energy of such anions is in the continuum (i.e., higher than for the system neutral + electron), and they can release the excess energy in several competing channels. The detachment of excess electrons is one of them. By analyzing the energies of the detached electrons, one can obtain information about both the initial state of the anion and the final states of the neutral. This reveals details of the nuclear dynamics that is involved in the relaxation process of the resonance.

There are several possibilities for how to prepare the temporary anions. One is by the collision of a free electron with a neutral molecule. The lifetime of such compound states can vary across many orders of magnitude.[1,2] It ranges from the background scattering (where the "lifetime" is usually just a flyby time and one typically does not use the word anion at all) to the formation of resonances with an electronic lifetime often in a femtosecond or picosecond timescale. A suitable experimental tool to probe such collisions is electron energy loss spectroscopy,[3] where a beam of electrons with controlled incident energy (ε_i) collides with a neutral target and the final energy of the scattered electron (ε_f) is recorded. The difference $\Delta\varepsilon = \varepsilon_i - \varepsilon_f$ is the energy loss. A neat extension of this traditional technique is the two-dimensional electron energy loss spectroscopy (2D EELS), where the energy loss spectra are recorded for many incident energies and thus provide a complex picture of the collision dynamics.[4,5] A different method of populating resonances is by photoexcitation of bound anions. Their formation strongly influences the electron detachment channel, and the

resonance footprints are thus manifested in the photoelectron spectra.[6] Here, a photon with controlled energy $h\nu$ collides with the anion and leads to an outgoing electron with the energy ε_f. The difference $\varepsilon_b = h\nu - \varepsilon_f$ is the electron binding energy. This method also can be performed in a two dimensional manner by recording photoelectron spectra over a range of incident photon energies.[7] Hence, 2D photoelectron spectroscopy is complementary to 2D electron energy loss spectroscopy. However, both methods have been developed in different communities and have not been compared in detail and such a comparison is an important part of the current study.

In both cases, electron energy loss spectroscopy and photoelectron spectroscopy, two basic types of vibrational excitation have been typically recognized. One is the excitation of specific vibrational modes with a constant energy loss (or constant binding energy): the energy of the emitted electrons is lower than the energy of the exciting particle by the vibrational quantum, which is left in the neutral molecule. The second common type is unspecific excitation: fast intramolecular vibrational excitation (IVR) leads to redistribution of excess energy among the vibrational degrees of freedom and slow (thermal) electrons are emitted over a wide range of excitation energies.[3] Few systems, however, show a third type of emission, where the electrons are emitted at constant finite final energies (i.e., not at constant energy loss or binding energy).[4,8–10] These energies correspond to de-excitation of specific vibrational modes and were detected in both photodetachment and electron-energy loss studies. Recently, we have identified a mechanism for such mode-specific vibrational autodetachment following the excitation of resonances in nitrobenzene.[11] In this paper, we provide details of vibrational excitation and electron emission from the excited anions in this molecule. We cover all observed types of electron emission.

Several aspects make nitrobenzene an interesting target from the point of view of electron collisions. It has a relatively high dipole moment of 4.22 Debye.[12] This leads to an existence of a dipole bound state with a binding energy of 28 meV.[13] The high dipole moment primarily motivated a number of electron elastic scattering studies, both experimental[14,15] and theoretical.[15,16] Also interesting is the structure of anion states. The LUMO of neutral nitrobenzene is $\pi^*(b_1)$. When an additional electron occupies this orbital, it creates a bound anion state with the adiabatic binding energy of 1.00 ± 0.01 eV.[13] Higher unoccupied orbitals of nitrobenzene give rise to resonances. The electron transmission experiment[17–19] located the resonances at 0.55, 1.36, 3.79, and 4.69 eV (with respect to the ground state of the neutral molecule). They can relax either via electron emission or via dissociation. In the latter case, these resonances give rise to a number of stable anionic fragments, as revealed by dissociative electron attachment spectroscopy.[19–21] Important for the present paper is the fact that electron attachment close to zero eV yields the non-dissociated anion NB^-, which was detected on the typical mass-spectrometric timescales, i.e., microseconds.

Our results provide detailed information about all the above-mentioned aspects of the electron–nitrobenzene interactions. Encoded in the electron spectra are the dynamics on resonant states, structural changes upon the electron attachment/detachment, role of long-range electron–molecule interaction (especially of the non-valence dipole-bound state), and high heat capacity leading to a long-living parent anion.

II. EXPERIMENT

A. Electron collision experiment (Prague)

The electron scattering experiments were performed using the electron energy loss spectrometer described earlier.[22,23] The electrons are emitted from a heated iridium filament and energy-selected by a double-hemispherical electron monochromator. They collide with the effusive beam of the nitrobenzene gas, and the energies of scattered electrons are analyzed with a double-hemispherical electron analyzer. The analyzer is rotatable, and the scattering angle can be additionally modified by a magnetic angle changer. The angle changing capacity was not used in the present measurements; all the data shown here were taken at the fixed mechanical scattering angle of 135°. The choice of this angle was determined by the fact that in electron scattering, the direct excitation processes related to direct-dipole excitation have cross sections peaking at small scattering angles.[24,25] The resonant processes that are of interest here are best visible in the backward scattering 180° angle. 135° is the highest mechanically accessible scattering angle in the present setup. The energy of the incident beam was calibrated on the 19.365 eV 2^2S resonance in helium. Combined electron-energy resolution was 17 meV, as determined from the width of the elastic peak.

B. Photodetachment experiment (Durham)

2D photoelectron (PE) spectroscopy was carried out using two separate instruments. The first employs a molecular beam source in which the vapor pressure of a drop of NB is entrained in Ar carrier gas (3 bars) and expanded into vacuum using a pulsed valve. The expansion was crossed by a 300 eV electron beam to generate NB^-.[26] In a second experiment, NB^- was generated using electrospray ionization.[27,28] In either experiment, NB^- was mass-selected using a time-of-flight mass-spectrometer and intersected with light from a tunable nanosecond (≈5 ns) Nd:YAG-pumped optical parametric amplifier (OPA) in a velocity-map imaging PE spectrometer.[26,29] The PE spectrometer was calibrated using iodide and had a resolution of <3% and <5% of ε_f for the molecular beam and electrospray ionization experiment, respectively. The difference in ion sources leads to a difference in the temperature of the anions: for the molecular beam, the internal energy is not equilibrated, but the typical vibrational temperature is <100 K; for the electrospray ionization source, the temperature is expected to be thermalized at ≈300 K. Below, we present only the results from the molecular beam source (higher resolution), but we note that very similar results were obtained at 300 K. Finally, we have also performed time-resolved photoelectron spectroscopy exciting the anion at 2.08 eV and probing the subsequent dynamics at 0.95 eV with an overall time-resolution of ~100 fs. Both pump and probe pulses were generated in separate OPAs: the 2.08 eV (595 nm) was generated by the second harmonic generation of the signal output of one OPA and the 0.95 eV (1300 nm) was the signal output of the second OPA. Both beams were combined collinearly and loosely focused in the interaction region.

III. RESULTS AND DISCUSSION

The electron energy loss experiment on nitrobenzene NB can be summarized as

$$e^-(\varepsilon_i) + \mathrm{NB} \rightarrow \mathrm{NB(exc)} + e^-(\varepsilon_f). \quad (1)$$

The photodetachment experiment can be summarized as

$$h\nu + \mathrm{NB}^- \rightarrow \mathrm{NB(exc)} + e^-(\varepsilon_f), \tag{2}$$

where $h\nu = \varepsilon_i - \varepsilon_b$ and NB(exc) indicates that NB is generated with some additional vibrational excitation. Figure 1(a) shows the two-dimensional electron impact and photodetachment spectra. The energies of the exciting particles (ε_i and $h\nu$) are varied, and at each of these energies, the kinetic energy spectrum of emitted electrons is recorded. The intensity is color-coded. There are a number of features visible in the 2D spectra, which will be discussed individually in the following subsections. The diagonal signals correspond to specific vibrational excitation (Sec. III A). The vertical features at low final energies correspond to mode-specific emission of constant-ε_f electrons (Sec. III B). Finally, the underlying broad background at low final energies is the unspecific vibrational excitation corresponding to statistical electron emission (Secs. III C and III D).

A. Specific vibrational excitation

The diagonal features in the 2D EELS spectra, Fig. 1(a), mean that the electron energy loss ($\Delta\varepsilon = \varepsilon_i - \varepsilon_f$) is constant. Similarly, in the 2D PE spectra, Fig. 1(b), they mean that the electron binding energy ($\varepsilon_b = h\nu - \varepsilon_f$) is constant. In both cases, they stand for the excitation of specific vibrational modes. The excited modes are easier to identify when the spectra are plotted in the traditional way [Fig. 1(c)]: as one-dimensional spectra where the signal is not a function of the outgoing electron energy ε_f, but rather a function of $\Delta\varepsilon$ or ε_b. These quantities directly express which vibrational modes are excited in the electron impact experiment and in the photodetachment experiment. Assignment of the modes was performed based on the vibrational analysis of infrared spectra in the literature[30,31] or by computational chemistry.

There is a clear difference in the excited modes in the two experiments. In photodetachment, across the whole $h\nu$ range, there is a dominant progression corresponding to the NO_2 symmetric stretch (166 meV). This is in agreement with the observation of

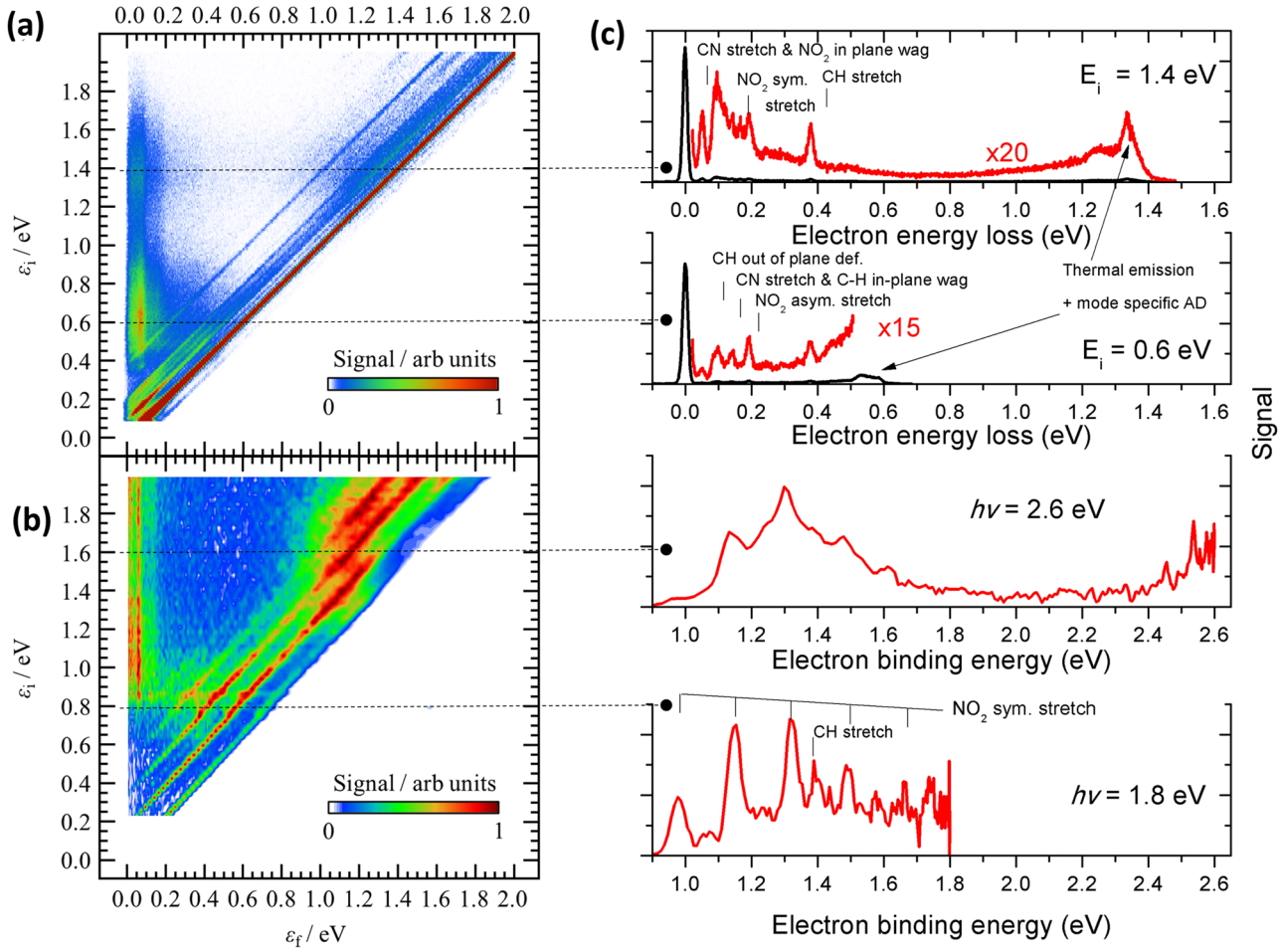

FIG. 1. (a) Two-dimensional electron-energy loss spectra of NB (top) and photodetachment electron spectra of NB^- (bottom). (b) Electron spectra at two different excitation energies for each experiment. (c) The horizontal scale of PE spectra is shifted with respect to that of EELS by 1 eV to account for the electron affinity of NB.

Desfracois *et al.*[13] and 2D PE spectroscopy of para-dinitrobenzene.[32] The main factor determining the direct vibrational excitation in photodetachment is the difference in the equilibrium molecular geometries of NB^- and NB. Both are planar with the C_{2v} symmetry. The main difference is in the NO bond length, which is 0.1 Å longer in the anion (value from the present B3LYP/aug-cc-pVDZ calculation). This causes the strong NO_2 symmetric stretch excitation upon detachment. In the electron-impact experiment, the efficiency of vibrational excitation is more sensitive to the presence of resonances. The excited vibrations thus reflect the geometry change between the neutral and resonant anion, and there is stronger variation of the excited modes with changing incident energy ε_i. At the incident energy of 1.4 eV, the dominant mode is the C–H out-of-plane deformation. As will be shown below, this falls in the region of the $\pi_2^*(b_1)$ resonance. It corresponds to the temporary occupation of the out-of-plane b_1 orbital (LUMO+2 of the neutral NB); it is thus not surprising that it excites modes breaking the planar symmetry. Quite strong is also the mode containing the C–NO_2 stretch (due to high molecular masses on its both sites, the C–N bond in NB has an unusually low frequency of 52 meV). The NO_2 symmetric stretch excitation is visible. That follows from the nodal structure of the b_1 (LUMO+2): both CN and NO bonds are weakened by the addition of the electron in this orbital. At the incident energy of 0.6 eV, the excitation of the C–H bending modes is weaker, and the NO_2 symmetric stretch is not visible in the spectrum.

In the electron-impact experiment, a convenient method of revealing resonances is by recording the excitation curves of individual vibrations. Experimentally, these are measured by scanning both the monochromator and the analyzer with their energy difference (energy loss) kept at a constant value. In principle, this corresponds to a diagonal intensity profile of the 2D EELS spectrum. Figure 2 shows the excitation curves of four different energy losses. Several features can be recognized. First, all excitation curves show threshold peaks of varying intensity. A peak at the threshold means that the electron efficiently excites the given vibration as soon as it has enough energy to do so, and this efficiency steeply decreases with increasing electron energy. Such vibrational excitation at the threshold is a well-known effect in electron collisions with polar molecules; the underlying physical principles are theoretically described, e.g., in the review by Itikawa.[24] There are four resonances visible in the excitation curves, marked by vertical bars in Fig. 2. The lowest one is at 0.49 eV. This is the $\pi_1^*(a_2)$ shape resonance, reported previously by the ETS (electron transmission spectroscopy) technique at 0.55 eV.[18] It is rather narrow. The width of the resonant peak in the excitation curve is determined by a combination of the resonance electronic width and the Franck–Condon overlap. The narrow peak thus suggests both a small resonant width and that the geometry of the resonant state in its energetic minimum is similar to that of the neutral NB.

The $\pi_2^*(b_1)$ shape resonance centered around 1.45 eV (in ETS it was reported at 1.5 eV[18]) is much broader. Additionally, there are two broad resonances, centered roughly around 3.8 and 4.9 eV. The first one (ETS value 3.79 eV) was assigned by Modelli and Venuti[18] to be a core-excited shape resonance. This might be the reason for its very weak footprint in the spectra, since the two-particle resonances are generally inefficient in the vibrational excitation, as will be detailed in Sec. III B. The last visible resonance at 4.9 eV (ETS value 4.69 eV) was assigned as $\pi_3^*(b_1)$ shape resonance.[18] Its effect on the vibrational excitation is rather weak, which may be caused by the fact that such high-lying shape resonance will necessarily have a large width. This leads to fast autodetachment prior to considerable nuclear motion of the transient anion.

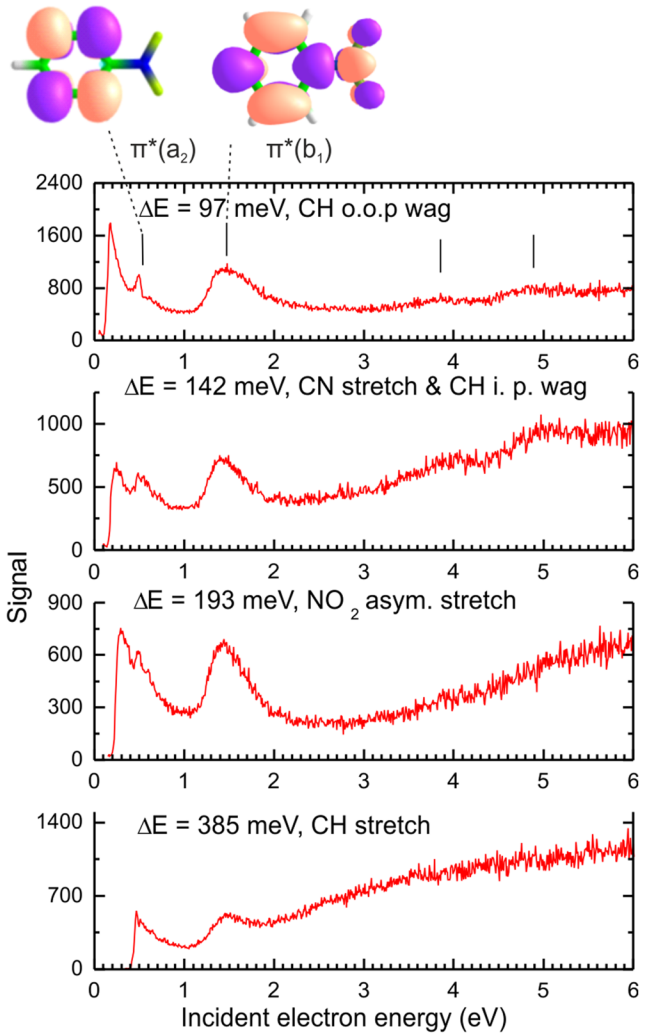

FIG. 2. Excitation curves of four energy losses in the electron collision experiment. The vertical bars denote the positions of resonances. Drawn on top are the isosurfaces of neutral NB orbitals (LUMO+1 and LUMO+2), the occupation of which gives rise to the two lowest shape resonances.

In the photodetachment experiment, the footprint of resonances is different. The most obvious signatures of resonances are changes in the excitation cross section as resonances are directly photoexcited. This would lead to changes in the overall electron yield as a function of photon energy. We have not performed such experiments in the present case. The second signature is in the properties of the outgoing electron. In direct detachment, the electron will leave according to the Franck–Condon factors between the anion and neutral. As resonances are excited, there is a finite lifetime of the resonance before the electron is emitted. Hence, nuclear motion can

take place on the resonance and Franck–Condon factors can change between the resonance and final neutral state. In Fig. 1, this is clearly apparent in the spectra shown at $h\nu$ = 1.8 and 2.6 eV, where the latter is resonant with the $\pi_2^*(b_1)$ resonance. While the vibrational modes of the NO_2 symmetric stretch remain visible, they are much less resolved and the Franck–Condon profile has shifted towards lower kinetic energy (higher binding energy). Note that the lower $\pi_1^*(a_2)$ resonance is not observed clearly in the high KE energy spectrum because photoexcitation to it from the HOMO is optically forbidden (although symmetry allowed).

An additional signature of resonance excitation can be gained from the photoelectron angular distributions.[6,7,9,33] These are sensitive to the molecular orbital from which the electron is detached, and, therefore, upon excitation of a resonance, this molecular orbital is different and often leads to corresponding changes in the outgoing electron's angular distribution. The angular distributions are typically quantified by an anisotropy parameter, β_2, which has values between +2 (corresponding to electron emission predominantly aligned with the polarization axis of the light) and −1 (corresponding to emission perpendicular to the polarization axis).[34] Figure 3 shows the 2D β_2 spectrum associated with the 2D PE spectrum in Fig. 1. This shows that the direct detachment from $\pi_2^*(b_1)$ has a $\beta_2 < 0$ and approaches −1. Such negative anisotropy is consistent with the direct photodetachment from a π molecular orbital.[35] Generally, β_2 is a slowly varying function of ε_f as differing partial waves interfere. This can be seen in Fig. 3 as β_2 becomes more negative as ε_i (or $h\nu$) increases in the range up to $\varepsilon_i \sim 0.6$ eV. However, at $\varepsilon_i \sim 1.0$ eV, there is a sudden change in β_2, which rapidly becomes $\beta_2 \sim 0$ as ε_i increases and then returns to negative values again for $\varepsilon_i > 1.6$ eV. The sudden change in β_2 coincides with the excitation of the $\pi_2^*(b_1)$ resonance and clearly demonstrates the sensitivity of β_2 to the changing molecular orbital involved in the electron emission process.

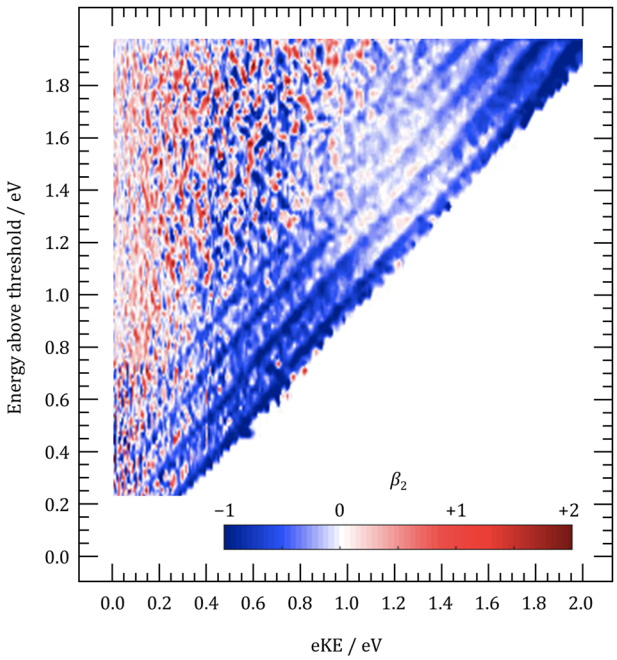

FIG. 3. Two-dimensional spectrum of the anisotropy parameter β_2 in the photodetachment experiment.

B. Mode-specific emission of constant ε_f electrons

The vertical features in both 2D spectra at $\varepsilon_f < 0.2$ eV correspond to specific excitation, however, in a different way than the diagonal features discussed above. Here, the electrons at constant final energies are emitted, which means that the emission process itself de-excites specific modes and the emitted electrons get a constant kinetic energy kick. When 1D spectra are plotted as a function of the emitted electron energy ε_f (Fig. 4), this type of emission is manifested as the peaks superimposed on a smooth background. We have recently provided a detailed analysis and explanation for this effect.[11] These electrons are not emitted directly from a resonant state. Rather, the resonance undergoes an internal conversion (or a series of these) to the ground state, and, eventually, the long-range dipole-bound state is populated. Upon the electron detachment from this non-valence state, specific vibrational modes are de-excited. The kinetic energy of these electrons corresponds to the vibrational energies of specific modes minus the binding energy of the dipole-bound state. The selection rules for such mode-specific detachment are based on the non-adiabatic coupling elements between the non-valence anion state and the final neutral state and have been discussed in detail previously.[11,36]

Here, we focus on the entrance channels to this emission in the electron scattering experiment. They are manifested in the type of

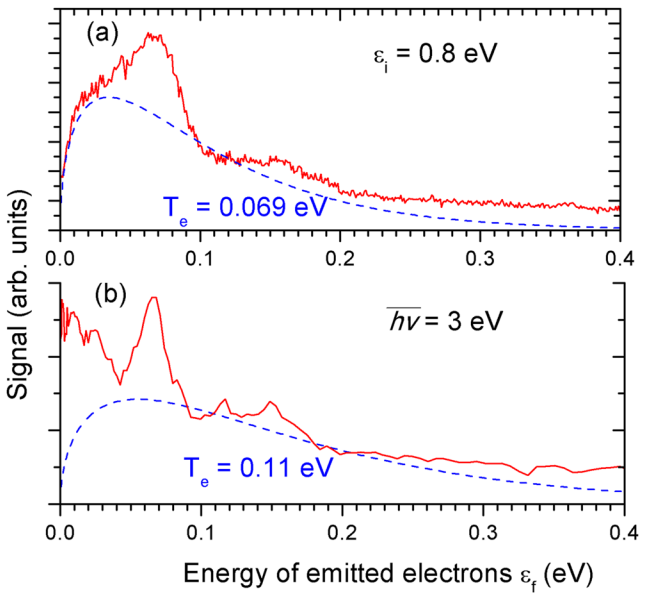

FIG. 4. Low-ε_f part of the spectrum of emitted electrons. (a) EELS experiment at ε_i = 0.8 eV. (b) Photodetachment experiment at a mean photon energy of 3 eV. This is the average of nine spectra taken between 2.9 and 3.1 eV photon energy with the step of 0.025 eV. Dashed line indicates the model for statistical electron emission, Eq. (8). The emission temperatures are T_e = 0.069 eV in (a) and 0.11 eV in (b).

measurement, where ε_f, which is let to pass the analyzer, is kept constant (in this case $\varepsilon_f = 0.07$ eV) and the incident energy ε_i is being scanned (Fig. 5). In principle, such a spectrum corresponds to the intensity profile along constant-ε_f in the 2D spectrum. The very high peak at $\varepsilon_i = 0.07$ eV (black trace) is the elastic signal. On the magnified red trace, one can see several narrow peaks below $\varepsilon_i \approx 0.5$ eV. These are the threshold electrons originating from the specific excitation. The additional broad peaks reveal at which incident energies the mode-specific emission sets in. We have marked positions of the two shape resonances as obtained from Fig. 2. Both of them are visible also in Fig. 5: the $\pi_1^*(a_2)$ 0.49 eV resonance as a narrow peak and the $\pi_2^*(b_1)$ 1.4 eV resonance as a broad band (with a center perhaps at a bit lower incident energy). However, the strongest band, centered around 0.65 eV, does not have any equivalent in the excitation curves in Fig. 2. We conclude that this has to be a Feshbach resonance. Feshbach resonances typically have long (picosecond) lifetimes before the electron is emitted, since such decay requires a change in the electronic configuration involving two electrons. Hence, these are rarely visible in the vibrational excitation curves such as those in Fig. 2. However, in the present case, such Feshbach resonance clearly undergoes an internal conversion to the ground anion state and emits electrons via the dipole-bound state. Indeed, we have computationally identified[11] a low-lying $^2B_2$ $(b_2^{-1}b_1^2)$ Feshbach resonance (vertically 1.25 eV above the neutral ground state).

Similar to the electron spectra of Fig. 1(a), the photoelectron spectra of Fig. 1(b) show that the mode-specific emission has an onset and that it remains present over a wide range of ε_i. The onset in the photoelectron spectra is at $\varepsilon_i \sim 0.8$ eV, which differs with that from the 2D EELS ($\varepsilon_i \sim 0.4$ eV). Moreover, as mentioned above, direct excitation to the $\pi_1^*(a_2)$ resonance is optically forbidden. Instead, calculations have shown that the above-mentioned $^2B_2$ Feshbach resonance may be optically excited.[11] This excitation is symmetry forbidden but is vibronically allowed through b_1 (out-of-plane) and b_2 (in-plane) vibrational modes. This transition has a very broad Franck–Condon profile, and the intensity can be borrowed to allow some excitation of the $\pi_1^*(a_2)$ resonance or indirect population of the $\pi_1^*(a_2)$ resonance may be possible through internal conversion. Its signature is not directly visible in the direct detachment as it is for the $\pi_2^*(b_1)$ resonance, which shows changes in the Franck–Condon factors and changes in β_2. Nevertheless, its presence is clearly evidenced by the onset of the mode-specific emission at low ε_f.

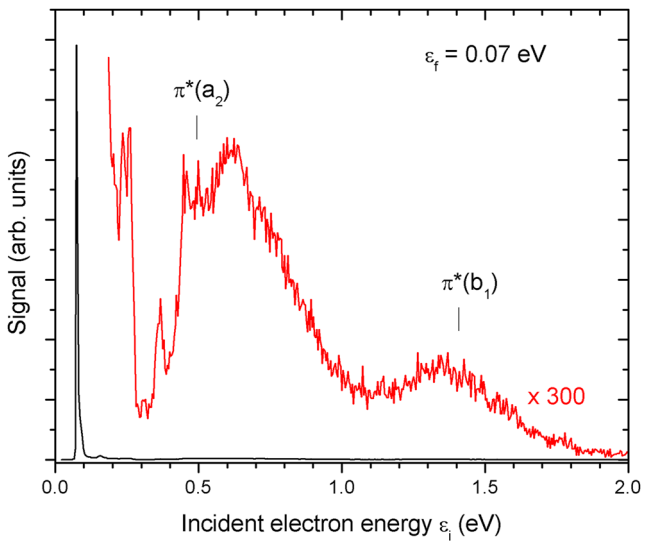

FIG. 5. Yield of electrons with a constant final energy of 0.07 eV in the electron collision experiment. The vertical bars mark positions of the two lowest shape resonances as obtained from Fig. 2.

C. Statistical electron emission

In both experiments, the mode-specific emission is superimposed on a smooth background signal, which is decreasing with increasing ε_f. This is a thermionic emission (also termed unspecific vibrational excitation): upon the resonance formation, the system relaxes to the anion ground state, and due to the fast intramolecular vibrational redistribution, the energy is randomized over the vibrational degrees of freedom. The electron is then emitted statistically. This is a common phenomenon.[37–40] In the following, we present a model for such emission, based on the detailed balance principle.[41,42]

The electron emission with kinetic energy ε can be described as

$$\mathrm{NB}^-(E_{int}) \rightarrow \mathrm{NB}(E_{int} - E_a - \varepsilon) + e^-(\varepsilon), \tag{3}$$

$$\text{parent} \rightarrow \text{daughter}. \tag{4}$$

The internal energy of the emitting anion E_{int} will be taken with respect to its ground electronic and vibrational state. In the case of photoexcitation, thus, $E_{int} = h\nu$, and in the case of electron collision, $E_{int} = \varepsilon_i + E_a$, where $E_a = 1$ eV is the electron affinity. The emission rate constant depends on the internal energy and on the energy of the emitted electron and is given by the Weisskopf formula,[41,42]

$$k(E_{int}, \varepsilon) = \frac{2m_e}{\pi^2\hbar^3}\sigma(\varepsilon)\varepsilon\frac{\rho_d(E_{int} - E_a)}{\rho_p(E_{int})}e^{-\frac{\varepsilon}{T_e}}. \tag{5}$$

Here, $\sigma(\varepsilon)$ is the cross section for the reverse process: electron attachment to neutral nitrobenzene. ρ_d and ρ_p are the densities of vibrational states of the daughter (neutral) and parent (anion) molecules, evaluated at their respective internal energy contents. Finally, T_e is the microcanonical electron emission temperature (in units of energy). This temperature is defined from the vibrational density of states of the daughter:

$$\frac{1}{T_e(E_{int})} = \left.\frac{d\ln(\rho_d(x))}{dx}\right|_{x=(E_{int}-E_a)}. \tag{6}$$

We approximate the electron attachment cross section $\sigma(\varepsilon)$ by the Vogt–Wannier threshold law for s-wave electron capture $\sigma(\varepsilon) \propto \varepsilon^{-1/2}$. This law strictly holds only for nonpolar molecules. Several more advanced approximations for the electron capture cross section with polar molecules have been developed[43,44] and thoroughly tested on the electron emission from nitroalkane anions.[45] It turns out that they influence the resulting ε_f distributions only at very low kinetic energies, up to few tens of meV.[45] We thus keep the simple ansatz for the cross section

$$\sigma(\varepsilon) = c_\sigma\varepsilon^{-1/2}. \tag{7}$$

The vibrational densities of states ρ_d and ρ_p were evaluated by using the Beyer–Swinehart algorithm in the harmonic approximation.[46] The frequencies of the 36 normal modes of both neutral and anions were evaluated at the B3LYP/aug-cc-pVDZ level; for the former, they agreed well with the experimental data.[30,31] The emission temperature (6) was evaluated as a derivative of the neutral level density. It is shown in Fig. 6(a) as a function of the anion internal energy.

After the ansatz for cross section (7), the rate constant as a function of emitted electron energy ε becomes

$$k(\varepsilon) = C\sqrt{\varepsilon}e^{-\frac{\varepsilon}{T_e}}, \tag{8}$$

with C being an arbitrary constant. This expression represents the expected distribution of emitted electrons. The calculated distributions are shown in Fig. 4 for two anion internal energies E_{int} = 1.8 and 3 eV. The corresponding emission temperatures [Fig. 6(a)] are T_e = 0.069 and 0.11 eV. The first distribution is compared with the result of the electron collision experiment at ε_i = 0.8 eV, and the second one is compared with the photoelectron spectrum at $\overline{h\nu}$ = 3 eV (average of the spectra between 2.9 and 3.1 eV). The model provides a very good estimate for the baseline of the spectrum, on top of which the mode-specific signal described in Sec. III B is superimposed. The agreement is worse for the photodetachment spectrum

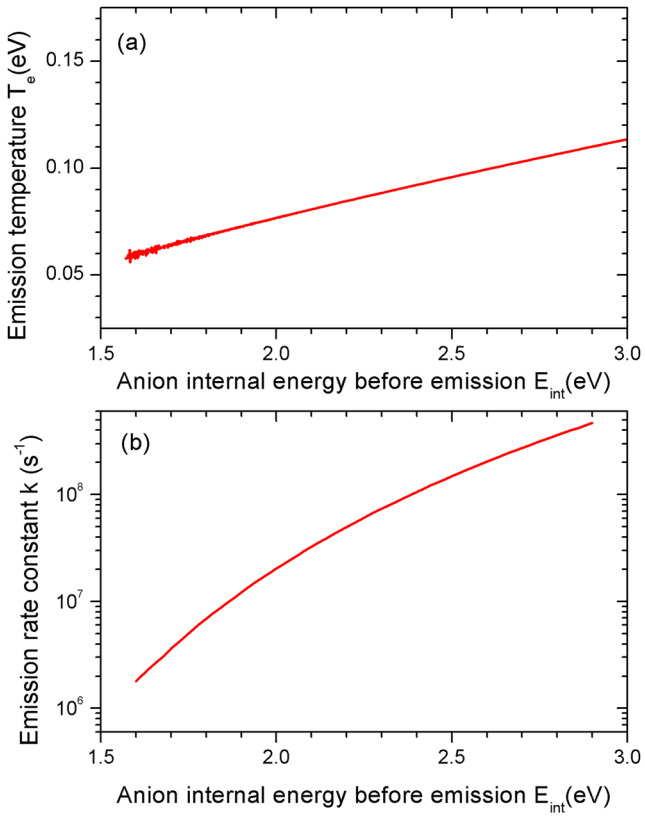

FIG. 6. Elements of the model for the statistical emission. (a) Emission temperature T_e, Eq. (6). (b) Emission rate constant k, Eq. (9). Both are plotted as a function of the internal energy of the NB anion prior to electron emission, E_{int}.

at very low emission energies, ε_f < 50 meV, where the model clearly underestimates the experimental data. The reason is that at low energies, the cross section for the reverse processes, electron attachment, may be much larger than the one resulting from the Vogt-Wannier law. A microscopic reversibility holds: if the inverse process, the electron attachment, is more effective, also the current process, the electron detachment, will be more effective. Due to this, the emission probability will in reality be much larger than the one resulting from the model. It should be noted that in the electron collision experiment, the response function of the hemispherical electron analyzer is difficult to control at such low energies; the drop of the experimental signal in Fig. 4(a) at low energies (and the resulting fortuitous agreement with the model) is thus an instrumental effect. The velocity-map imaging analyzer used in the photodetachment experiment provides much more reliable information about the low-energy emission.

We can even evaluate the absolute value of the statistical emission rate constant and its dependence on the anion internal energy. Integrating the rate constant (5) through all emitted energies, we obtain

$$k(E_{int}) = \int_0^\infty k(E_{int},\varepsilon)d\varepsilon = \frac{m_e}{\pi^2\hbar^3}c_\sigma\sqrt{\pi T_e^3}\frac{\rho_d(E_{int}-E_a)}{\rho_p(E_{int})}. \tag{9}$$

We already have all the quantities on the right-hand side apart from c_σ. We can estimate it from the literature data on electron attachment rate constants. We use a quantitative comparison with sulfur hexaflouride. SF_6 follows the Wogt-Vannier law very well.[47] From its electron attachment cross section measured in a high-resolution experiment,[47] we estimate that $c_\sigma(SF_6) \approx 80$ Å^2 $\sqrt{\text{eV}}$. The thermal electron attachment rate constant for NB, as measured in a pulsed-Townsend experiment, is 0.017 times that of SF_6.[20] We will thus use $c_\sigma = 0.017c_\sigma(SF_6)$. Figure 6(b) shows the calculated value of $k(E)$. The inverse of $k(E)$ gives a typical timescale for the statistical emission. We probed it as described in Sec. III D.

D. Time-resolved (ns) electron collision experiment

We have experimentally probed the timescale for the statistical electron emission by pulsing the electron collision experiment. Figure 7(a) shows the electron spectrometer with the marked positions of the electrodes on which we superimposed the pulsing. The purpose of the pulsing was to open the monochromator (MONO) and analyzer (ANA) only for a certain time and to control the delay between the open periods. Different electrodes were chosen for gating in MONO and ANA. Ideally, the exit slit of the monochromator second hemisphere would be gated on the MONO side (symmetrical to that of ANA), since this would open the beam as close as possible to the interaction region, thus allowing for the best control of the interaction time. However, it turned out that pulsing this slit leads to strong deterioration of the incident electron beam resolution. We thus pulsed the MONO entrance slit, before the first MONO hemisphere. On the analyzer side, it was possible to gate the entrance slit (just after the collision region), and it turned out to be impossible to gate the exit slit since this led to the pickup of the pulsing signal by the channeltron.

Figure 7(b) shows the pulsing scheme. The delay between closing the MONO entrance slit and opening the ANA entrance slit was set to 200 ns. The electron travel time between the MONO gating

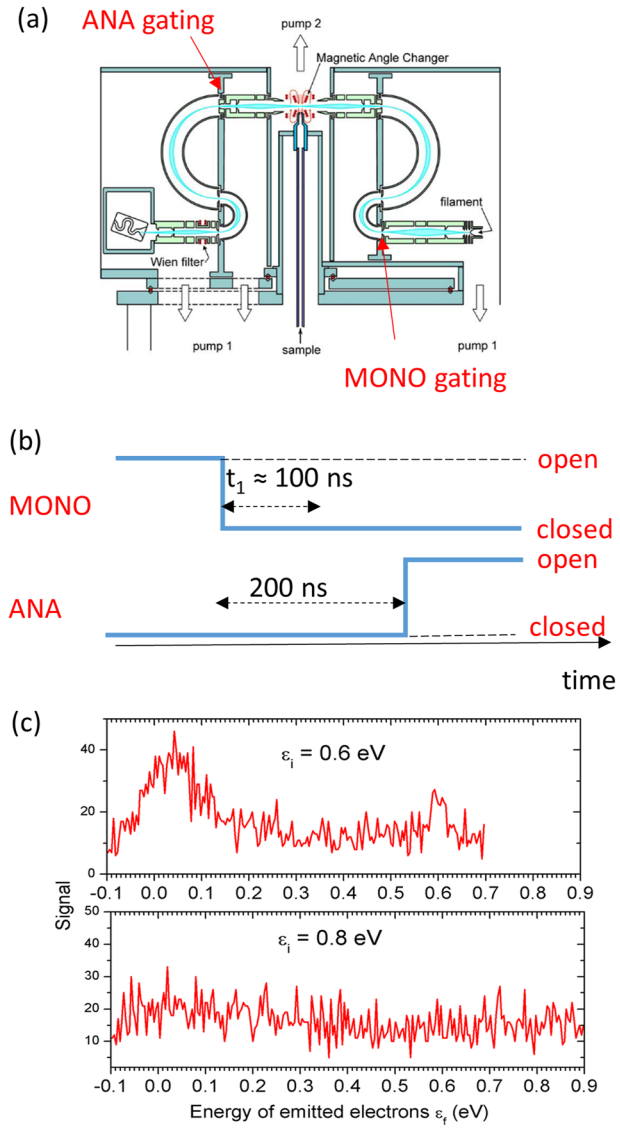

FIG. 7. (a) Scheme of the electron energy loss spectrometer with marked positions of the gated electrons on the monochromator (MONO) and analyzer (ANA) sites. (b) Pulse timing. The pulses are floating on the potentials of the two corresponding electrodes. The interval t_1 denotes the approximate electron travel time from the MONO gated electrode to the collision region. The pulsing repetition rate was 50 kHz. (c) Spectra of emitted electrons recorded at two different incident energies in the pulsed mode.

electrode and the collision region was $t_1 \approx 100$ ns (this is determined primarily by the pass energy through the hemispheres, which was 4 eV). The minimum delay window was thus ~100 ns. This means that only the electrons emitted later than 10^{-7} s after the e^- + NB collision were detected. Any electrons emitted faster are blocked and do not enter the analyzer. The repetition rate of the experiment was 50 kHz. We have verified the proper closing of the electrodes by the electron scattering from helium, and no elastic signal has been detected when the electrodes were pulsed as shown in Fig. 7(b).

Figure 7(c) shows spectra of delayed electrons upon electron scattering from nitrobenzene at two incident electron energies, 0.6 and 0.8 eV. While at lower incident energy, a clear signal of slow electrons is detected, the spectrum at 0.8 eV shows hardly any discernible signal in the present S/N ratio. Clearly, at $\varepsilon_i = 0.8$ eV ($E_{int} = 1.8$ eV), the anion is too hot, and the electrons are emitted in a time shorter than 100 ns. This is in surprisingly good agreement with the calculated emission rate constant $k(E_{int})$ from the statistical model, Fig. 6(b). The two incident electron energies correspond to anion internal energies of 1.6 and 1.8 eV. The calculated rate constant values are 1.8×10^6 and 6.9×10^6 $s^{-1,}$ with the corresponding characteristic emission lifetimes of 555 and 144 ns, respectively. Considering the approximations used in the model and the steep dependence of the rate constant on the internal energy, these values are in good agreement with the experimentally observed 100 ns cutoff between the two incident energies.

Ideally, in this type of experiment, one would explore the dependence of the signal on the pulsing delay and incident energy in detail. However, as is apparent from Fig. 6(c), the signals are extremely low, and the long acquisition time prevents such systematic probing of the statistical emission.

We could perform an analogous measurement in the photoelectron experiment.[48,49] Specifically, the multichannel plates that amplify the electron signals were gated using a pulse of ~200 ns duration so that the electron signal was only observed over this 200 ns window. Upon delaying this gate with respect to the laser interacting with the ion packet by >200 ns, we observed essentially no signal. This suggests a lifetime of the thermionic emission that is shorter than ~200 ns, consistent with the predictions above.

E. Competition between statistical and mode-specific detachment from the dipole-bound state: Reverse valence to non-valence state internal conversion

From Figs. 1 and 5, it is clear that both statistical and mode-specific emissions via a dipole-bound state are taking place following the excitation of resonances. The involvement of the dipole-bound state can come about in two ways. First, it is conceivable that the π^* resonances undergo internal conversion to form the non-valence dipole-bound state. Such a process has been observed in a number of molecular[10,50] and cluster[51–53] anions through time-resolved photoelectron imaging. Indeed, the spectral signature of the subsequent emission is similar to that observed here.[10] However, such valence to non-valence internal conversion typically occurs only in an energy range close to the threshold, where the valence resonance and non-valence states are close in energy. In the present case, it is striking that the range over which the mode-specific vibrational autodetachment from the dipole-bound state can be seen is so large (indeed, we have extended the PE spectra to higher $h\nu$, and this channel remains visible beyond 3 eV into the continuum). Furthermore, we have performed time-resolved PE spectroscopy in an attempt to observe a transiently populated dipole-bound state but could not observe any signal from this state over the first few picoseconds.

A second possible mechanism (Fig. 8) relates to the observation that the valence π^* resonances decay to form the ground electronic

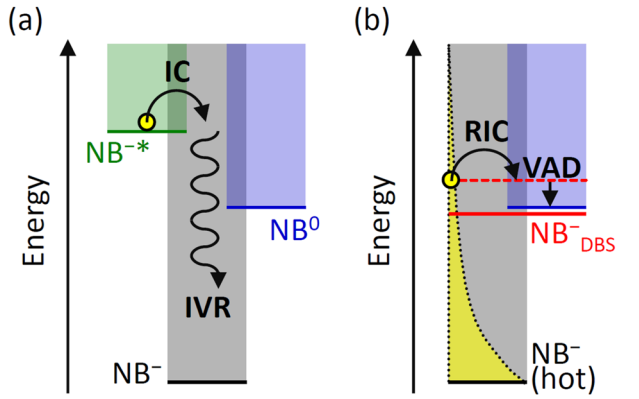

FIG. 8. Jabłoński-type diagram of the proposed mechanism for the mode-specific vibrational autodetachment. (a) The resonance $NB^{-}*$ is initially excited and undergoes internal conversion (IC) to form the anion ground state, NB^{-}, and the energy is subsequently redistributed via IVR. (b) The hot NB^{-} then populates the vibrational Feshbach resonances of the dipole bound state (DBS) via a reverse internal conversion (RIC) mechanism, and the electron subsequently undergoes (mode-specific) vibrational autodetachment (VAD).

state of the anion. We know this occurs because of the statistical emission that is seen [Figs. 4 and 7(c)].[48,54] The statistical emission requires IVR to populate modes that can detach an electron. Hence, by definition, such excited modes have energies that lie in the vicinity of the detachment threshold and, hence, can degenerate with the dipole-bound state. We, therefore, suggest that the dipole-bound state can become populated through a reverse internal conversion from the vibrationally hot ground electronic state of NB^{-} to the non-valence state. Such a reverse valence to non-valence internal conversion is consistent with our time-resolved PE spectra, which showed no transient dipole-bound state as this would only be populated over the thermionic emission lifetime (see Sec. III D) and once populated is likely to decay within a few picoseconds. Hence, observing this population in a time-resolved PE measurement, which currently has a maximal range of <1 ns, is not possible; the dynamics would need to be monitored over a longer timescale as suggested in Secs. III C and III D.

The newly proposed mechanism is not without precedence. Reverse intersystem crossing is responsible for thermally activated delayed fluorescence (TADF), which has had a major impact on organic light emitting diode research.[55–57] In this process, a triplet state populates a singlet state, which is higher in energy, which subsequently emits light to overcome the 25% conversion limit imposed by the presence of both singlets and triplets.[58] A second related example is recurrent or Poincaré fluorescence, in which internal conversion from an excited state leads to a hot ground state that subsequently populates the lowest lying singlet excited state through reverse internal conversion, and this excited state subsequently fluoresces.[59–61] This mechanism has been suggested to account for the formation of certain anions in the interstellar medium, such as PAHs and polyyenes.[61] The new mechanism described here is similar in spirit to recurrent fluorescence; however, rather than radiative loss, the energy is emitted by non-radiative electron emission. Additionally, the reverse internal conversion is not between two valence states but involves a reverse valence to non-valence transition. To the best of our knowledge, this mechanism has not been described previously.

IV. CONCLUSIONS

In conclusion, we probed the electron emission from nitrobenzene transient anions using both electron energy loss spectroscopy and photoelectron spectroscopy. In the first one, the starting geometry of the molecular framework is that of the neutral; in the second one, it is that of the anion. Some aspects of the resulting electron emission are strongly influenced by this difference, while some are common in the two cases. The difference is primarily reflected in the excitation of specific vibrational modes. Here, the photodetachment dominantly excites the NO_2 symmetric stretch and its overtones; the electron collisions primarily excite the out-of-plane bending modes, the CN stretch and the NO_2 asymmetric stretch. Electronic resonances present in the system leave clear footprints in both spectroscopies: they are visible in the electron impact excitation curves of individual vibrations, broadening of the photodetachment Franck–Condon profiles, or photoelectron angular distributions.

Other types of electron emission differ very little in the two experiments. One is the mode-specific emission of slow electrons mediated by the presence of the dipole-bound state. The present spectra identify the entrance channels for this process, the most prominent in both experiments being the formation of the $^2B_2$ Feshbach resonance. Both experiments also reveal the presence of electrons that are statistically emitted from vibrationally hot ground state anions. A model based on the detailed balance principle describes this emission very well. Finally, the mode-specific emission from the dipole-bound state has been explained through a new mechanism involving a reverse valence to non-valence internal conversion.

ACKNOWLEDGMENTS

This work was supported by Czech Science Foundation Project No. 20-11460S, the European Research Council (Grant No. 306536), and the EPSRC (EP/M507854/1).

AUTHOR DECLARATIONS

Conflict of Interest

The authors have no conflicts to disclose.

Author Contributions

Miloš Ranković: Data curation (equal); Investigation (equal); Writing – review & editing (equal). **Pamir Nag**: Data curation (equal); Formal analysis (equal). **Cate S. Anstöter**: Data curation (equal); Formal analysis (equal). **Golda Mensa-Bonsu**: Data curation (equal); Formal analysis (equal). **T. P. Ragesh Kumar**: Data curation (equal); Formal analysis (equal). **Jan R. R. Verlet**: Conceptualization (equal); Supervision (equal); Writing – original draft (equal). **Juraj Fedor**: Conceptualization (equal); Writing – original draft (equal).

DATA AVAILABILITY

The data that support the findings of this study are available from the corresponding authors upon reasonable request.

REFERENCES

[1] H. Hotop, M.-W. Ruf, M. Allan, and I. I. Fabrikant, Adv. At. Mol. Opt. Phys. **49**, 85 (2003).
[2] I. I. Fabrikant, S. Eden, N. J. Mason, and J. Fedor, Adv. At. Mol. Opt. Phys. **66**, 545 (2017).
[3] M. Allan, J. Electron Spectrosc. Relat. Phenom. **48**, 219 (1989).
[4] K. Regeta and M. Allan, Phys. Rev. Lett. **110**, 203201 (2013).
[5] J. Dvořák, M. Rankovi, K. Houfek, P. Nag, R. Čurík, J. Fedor, and M. Čížek, Phys. Rev. Lett. **129**, 013401 (2022).
[6] C. W. West, J. N. Bull, E. Antonkov, and J. R. R. Verlet, J. Phys. Chem. A **118**, 11346 (2014).
[7] C. S. Anstöter, J. N. Bull, and J. R. R. Verlet, Int. Rev. Phys. Chem. **35**, 509 (2016).
[8] M. Allan, M. Lacko, P. Papp, Š. Matejčík, M. Zlatar, I. I. Fabrikant, J. Kočišek, and J. Fedor, Phys. Chem. Chem. Phys. **20**, 11692 (2018).
[9] G. Mensa-Bonsu, A. Lietard, D. J. Tozer, and J. R. R. Verlet, J. Chem. Phys. **152**, 174303 (2020).
[10] J. R. R. Verlet, C. S. Anstöter, J. N. Bull, and J. P. Rogers, J. Phys. Chem. A **124**, 3507 (2020).
[11] C. S. Anstöter, G. Mensa-Bonsu, P. Nag, M. Ranković, R. Kumar T. P., A. N. Boichenko, A. V. Bochenkova, J. Fedor, and J. R. R. Verlet, Phys. Rev. Lett. **124**, 203401 (2020).
[12] R. D. Nelson, D. R. Lide, and A. A. Maryott, *Selected Values of Electric Dipole Moments for Molecules in the Gas Phase*, National Standard Reference Data Series (National Bureau of Standards, 1967).
[13] C. Desfrançois, V. Périquet, S. A. Lyapustina, T. P. Lippa, D. W. Robinson, K. H. Bowen, H. Nonaka, and R. N. Compton, J. Chem. Phys. **111**, 4569 (1999).
[14] S. L. Lunt, D. Field, J.-P. Ziesel, N. C. Jones, and R. J. Gulleye, Int. J. Mass Spectrom. **205**, 197 (2001).
[15] L. Álvarez, F. Costa, A. I. Lozano, J. C. Oller, A. Muñoz, F. Blanco, P. Limão-Vieira, R. D. White, M. J. Brunger, and G. García, Phys. Chem. Chem. Phys. **22**, 13505 (2020).
[16] L. S. Maioli and M. H. F. Bettega, J. Chem. Phys. **147**, 164305 (2017).
[17] D. Mathur and J. B. Hasted, J. Phys. B: At. Mol. Phys. **9**, L31 (1976).
[18] A. Modelli and M. Venutti, Int. J. Mass Spectrom. **205**, 7 (2001).
[19] N. L. Asfandiarov, S. A. Pshenichnyuk, V. G. Lukin, I. A. Pshenichnyuk, A. Modelli, and Š. Matejčik, Int. J. Mass Spectrom. **264**, 22 (2007).
[20] R. N. Compton, L. G. Christophorou, G. S. Hurst, and P. W. Reinhard, J. Chem. Phys. **45**, 4636 (1966).
[21] A. Pelc, P. Scheier, and T. D. Märk, Vacuum **81**, 1180 (2007).
[22] M. Allan, J. Phys. B: At., Mol. Opt. Phys. **25**, 1559 (1992).
[23] M. Allan, J. Phys. B: At., Mol. Opt. Phys. **38**, 3655 (2005).
[24] Y. Itikawa, Int. Rev. Phys. Chem. **16**, 155 (1997).
[25] I. I. Fabrikant, J. Phys. B: At., Mol. Opt. Phys. **49**, 222005 (2016).
[26] J. P. Rogers, C. S. Anstöter, J. N. Bull, B. F. E. Curchod, and J. R. R. Verlet, J. Phys. Chem. A **123**, 1602 (2019).
[27] J. Lecointre, G. M. Roberts, D. A. Horke, and J. R. R. Verlet, J. Phys. Chem. A **114**, 11216 (2010).
[28] L. H. Stanley, C. S. Anstöter, and J. R. R. Verlet, Chem. Sci. **8**, 3054 (2017).
[29] D. A. Horke, G. M. Roberts, J. Lecointre, and J. R. R. Verlet, Rev. Sci. Instrum. **83**, 063101 (2012).
[30] J. H. S. Green and D. J. Harrison, Spectrochim. Acta, Part A **26**, 1925 (1970).
[31] L. S. Khaikin, I. V. Kochikov, O. E. Grikina, D. S. Tikhonov, and E. G. Baskir, Struct. Chem. **26**, 1651 (2015).
[32] C. S. Anstöter, T. E. Gartmann, L. H. Stanley, A. V. Bochenkova, and J. R. R. Verlet, Phys. Chem. Chem. Phys. **20**, 24019 (2018).
[33] T.-C. Jagau, D. B. Dao, N. S. Holtgrewe, A. I. Krylov, and R. Mabbs, J. Phys. Chem. Lett. **6**, 2786 (2015).
[34] K. L. Reid, Annu. Rev. Phys. Chem. **54**, 397 (2003).
[35] A. Sanov, Annu. Rev. Phys. Chem. **65**, 341 (2014).
[36] J. Simons, J. Am. Chem. Soc. **103**, 3971 (1981).
[37] M. Ranković, P. Nag, M. Zawadzki, L. Ballauf, J. Żabka, M. Polášek, J. Kočišek, and J. Fedor, Phys. Rev. A **98**, 052708 (2018).
[38] R. Kumar T. P., J. Kočišek, K. Bravaya, and J. Fedor, Phys. Chem. Chem. Phys. **22**, 518 (2020).
[39] A. Chachereau, J. Fedor, R. Janečková, J. Kočišek, M. Rabie, and C. M. Franck, J. Phys. D: Appl. Phys. **49**, 375201 (2016).
[40] M. Rankovic, T. P. R. Kumar, P. Nag, J. Kocisek, and J. Fedor, J. Chem. Phys. **152**, 244304 (2020).
[41] K. Hansen, *Statistical Physics of Nanoparticles in the Gas Phase* (Springer, 2013).
[42] J. U. Andersen, E. Bonderup, and K. Hansen, J. Phys. B: At., Mol. Opt. Phys. **35**, R1 (2002).
[43] I. I. Fabrikant and H. Hotop, Phys. Rev. A **63**, 022706 (2001).
[44] K. Hansen, Int. J. Mass Spectrom. **438**, 142 (2019).
[45] C. L. Adams, K. Hansen, and J. M. Weber, J. Phys. Chem. A **123**, 8562 (2019).
[46] T. Beyer and D. F. Swinehart, Commun. ACM **16**, 379 (1973).
[47] M. Braun, S. Marienfeld, M.-W. Ruf, and H. Hotop, J. Phys. B: At., Mol. Opt. Phys. **42**, 125202 (2009).
[48] J. N. Bull, C. W. West, and J. R. R. Verlet, Chem. Sci. **6**, 1578 (2015).
[49] J. N. Bull, C. W. West, and J. R. R. Verlet, Phys. Chem. Chem. Phys. **17**, 32464 (2015).
[50] J. N. Bull, C. S. Anstöter, and J. R. R. Verlet, Nat. Commun. **10**, 5820 (2019).
[51] J. N. Bull, C. W. West, and J. R. R. Verlet, Chem. Sci. **7**, 5352 (2016).
[52] J. N. Bull and J. R. R. Verlet, Sci. Adv. **3**, e1603106 (2017).
[53] J. P. Rogers, C. S. Anstöter, and J. R. R. Verlet, J. Phys. Chem. Lett. **9**, 2504 (2018).
[54] D. A. Horke, Q. Li, L. Blancafort, and J. R. R. Verlet, Nat. Chem. **5**, 711 (2013).
[55] A. Endo, M. Ogasawara, A. Takahashi, D. Yokoyama, Y. Kato, and C. Adachi, Adv. Mater. **21**, 4802 (2009).
[56] H. Uoyama, K. Goushi, K. Shizu, H. Nomura, and C. Adachi, Nature **492**, 234 (2012).
[57] Z. Yang, Z. Mao, Z. Xie, Y. Zhang, S. Liu, J. Zhao, J. Xu, Z. Chi, and M. P. Aldred, Chem. Soc. Rev. **46**, 915 (2017).
[58] M. K. Etherington, J. Gibson, H. F. Higginbotham, T. J. Penfold, and A. P. Monkman, Nat. Commun. **7**, 13680 (2016).
[59] C. A. Parker and C. G. Hatchard, Trans. Faraday Soc. **57**, 1894 (1961).
[60] A. Léger, P. Boissel, and L. d'Hendecourt, Phys. Rev. Lett. **60**, 921 (1988).
[61] V. Chandrasekaran, B. Kafle, A. Prabhakaran, O. Heber, M. Rappaport, H. Rubinstein, D. Schwalm, Y. Toker, and D. Zajfman, J. Phys. Chem. Lett. **5**, 4078 (2014).